AIP | Applied Physics Letters

Fidelity imaging for atomic force microscopy

Sayan Ghosal and Murti Salapaka

Citation: Applied Physics Letters **106**, 013113 (2015); doi: 10.1063/1.4905633
View online: http://dx.doi.org/10.1063/1.4905633
View Table of Contents: http://scitation.aip.org/content/aip/journal/apl/106/1?ver=pdfcov
Published by the AIP Publishing

Fidelity imaging for atomic force microscopy

Sayan Ghosal[a] and Murti Salapaka[b]
Nanodynamics Systems Laboratory, Department of Electrical and Computer Engineering, University of Minnesota, Minneapolis, Minnesota 55455, USA

(Received 22 July 2014; accepted 26 December 2014; published online 7 January 2015)

Atomic force microscopy is widely employed for imaging material at the nanoscale. However, real-time measures on image reliability are lacking in contemporary atomic force microscopy literature. In this article, we present a real-time technique that provides an image of fidelity for a high bandwidth dynamic mode imaging scheme. The fidelity images define channels that allow the user to have additional authority over the choice of decision threshold that facilitates where the emphasis is desired, on discovering most true features on the sample with the possible detection of high number of false features, or emphasizing minimizing instances of false detections. Simulation and experimental results demonstrate the effectiveness of fidelity imaging. © *2015 AIP Publishing LLC*.
[http://dx.doi.org/10.1063/1.4905633]

Since its invention, the atomic force microscopy (AFM)[1] has led to fundamental discoveries and insights into the nature of matter. Many operational modes have evolved[2] over the last two decades which enable probing of matter with sub-nanometer resolution and with high speeds. Different methods suitable for soft-matter investigation are currently being researched where multiple modes of the cantilever flexure and multi-frequency excitation are being employed. Such methods hold the promise of further improvements in resolution and speed.[3] Even though performance of AFMs, for example, with respect to speed and resolution, have continuously improved, a key challenge of quantifying the goodness of measurements has remained largely unaddressed. As AFMs are metrological tools, AFM based images should be accompanied by confidence measures on the quality of the image.

Determining fidelity of AFM images is a difficult problem where many sources can contribute to the spurious interpretation of images acquired.[4] In particular, in methods where the cantilever is excited externally, the dynamics of the cantilever under the influence of the sample can be complex, where extraction of sample properties from measured signals becomes difficult. Typically, it is possible to adapt the operational parameters of imaging to lessen spuriousness; however, such a step has to be preceded with a means (see Fig. 1) to detect artifacts in the image. Moreover different AFM studies have varying demands on fidelity. Indeed, in many AFM studies, the sample being imaged is scanned in an exploratory phase, where the purpose is to detect features of interest. The exploratory phase is followed by a second phase, where features are probed more finely. In the exploratory phase, the detection of possible features has to be emphasized, whereas, in the second phase, it is important for detected features to have a high probability of being true.

In this letter, a measure on the fidelity of images obtained using dynamic mode operation of the AFM is devised. The fidelity measure can be determined faster than the time-scale of image-acquisition and is thus a real-time measure. Furthermore, the letter provides a control mechanism which can be used to strike a desired compromise between detection of true features versus lessening detection of false features. Methods developed are evaluated experimentally to assess their effectiveness. In the letter, it is assumed that a one-mode approximation of the cantilever flexure is sufficient and that the higher modes are not excited. A single mode approximation of the cantilever is described by

$$\frac{dp}{dt} = v; \quad \frac{dv}{dt} = -\frac{\omega_0}{Q} v - \omega_0^2 p + g(t) + \eta + \Phi(p, v), \quad (1)$$

where ω_0 is the first modal resonant frequency, Q is the quality factor, g is the external forcing, and η represents thermal noise. Here, Φ represents the tip-sample interaction force which depends on both the tip-position, p and tip-velocity, v. In many prevalent dynamic modes of operation, the external forcing $g(t)$ is sinusoidal with frequency close to the resonant

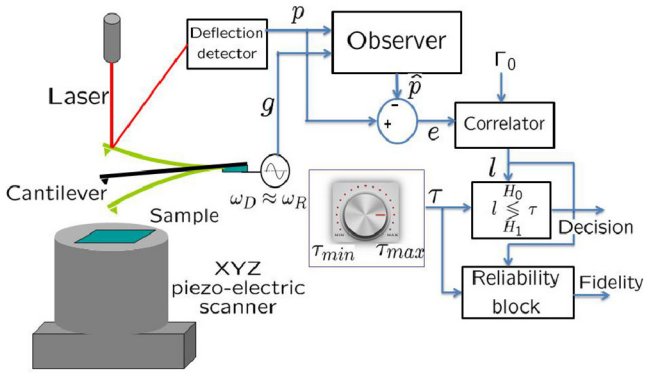

FIG. 1. Schematic diagram of the fidelity imaging architecture. In dynamic mode of operation, the cantilever is excited at the drive frequency ω_D, which is the same or very near the first modal resonant frequency of the cantilever ω_0. The observer accepts cantilever excitation g and the deflection signal p as inputs and generates estimated deflection $\hat{p}$. The tracking error $e = p - \hat{p}$ is processed by the correlator block to synthesize the likelihood signal l, which in turn is used for decision imaging and creating the fidelity metric. The decision threshold τ is varied in accordance with users' priority on detecting either most of the true sample features or the absence of features.

[a]Electronic mail: ghos0087@umn.edu
[b]Electronic mail: murtis@umn.edu

frequency ω_0 of the cantilever flexure; here, such a forcing will be assumed.

The real-time aspects of the fidelity measure rely on the concept of an *observer* (see Ref. 5), which provides estimates $\hat{p}$ and $\hat{v}$ of position p and velocity v of the cantilever, respectively. An observer provides these estimates by emulating the dynamics of a cantilever described by (1) with the assumption that the sample interaction is absent. Furthermore, the observer dynamics includes an additional correction term proportional to the error in estimating the position that forces the time derivatives of estimated position and estimated velocity. The observer dynamics is described by

$$\begin{aligned}\frac{d\hat{p}}{dt} &= \hat{v} + \underbrace{\ell_1(y-\hat{p})}_{correction};\\ \frac{d\hat{v}}{dt} &= -\frac{\omega_0}{Q}\hat{v} - \omega_0^2\hat{p} + g(t) + \underbrace{\ell_2(y-\hat{p})}_{correction}.\end{aligned} \tag{2}$$

Here, $y = p + \vartheta$ represents the measurement of the cantilever position, where ϑ is the noise introduced in measuring the cantilever deflection. The observer (2) is realized digitally which takes as inputs the measurement y of the cantilever deflection and the forcing g and yields as outputs estimates $\hat{p}$ and $\hat{v}$ of position p and velocity v, respectively.

The observer dynamics mimics the cantilever dynamics well when the sample interaction is absent (that is $\Phi = 0$ in (1)). Even when the sample is absent, the cantilever and observer states can be different caused by the mismatch in the initial conditions of the cantilever and the observer. Here, the cantilever position is being measured—however, the velocity is not, and thus, it is not possible to initialize the observer states to the cantilever states. The correction terms $\ell_1(y-\hat{p})$ and $\ell_2(y-\hat{p})$ with proper choice of ℓ_1 and ℓ_2 speed up the convergence of estimate $\hat{p}$ and estimate $\hat{v}$ to the cantilever's position p and velocity v, respectively. Thus, even if there is an initial mismatch between the cantilever's position and velocity and their estimates, the mismatch will be small within a cycle of the cantilever oscillation when the sample interaction is absent. The fast erasure of initial condition mismatch between the cantilever's state and the observer state provides the real-time capability of the fidelity measure. Indeed, in dynamic mode operation of the AFM, oscillation amplitudes of 20 nm and above are employed. Thus, the cantilever tip interacts only intermittently with the sample, once every cycle of oscillation and spends only a small fraction of the cycle under appreciable influence of the sample. During the rest of the cycle, the cantilever is mostly free of the interaction from the sample. The small interaction time with the sample allows for modeling the sample's influence as a reset of the cantilever position and velocity to new values. Immediately after the reset, there is no sample interaction; however, the observer state ($\hat{p}$ and $\hat{v}$) will be mismatched with the cantilever state (p and v), which is reset due to the previous contact with the sample. As described earlier, this mismatch rapidly vanishes, and, until the next contact with the sample, the observer state and the cantilever state are in sync, where any difference is due to noise (thermal noise η and measurement noise ϑ).

Summarizing the discussion above, in a dynamic mode operation where the cantilever comes into contact with the sample intermittently at most once every oscillation cycle, each such contact generates a short-lived mismatch between the cantilever and observer states. In particular, a measurement of the mismatch between the cantilever position and its estimate $\hat{p}$ is provided by $e := y - \hat{p}$. When there is no sample interaction ($\Phi = 0$), the cantilever and observer dynamics (1) and (2) are both linear, and thus, the response of the initial condition mismatch (say ν) can be determined in closed-form in terms of the parameters ω_0, Q, ℓ_1, and ℓ_2 and will be linear in ν.

Thus, assuming that the data are digitally sampled, an impulsive impact with the sample (leading to a reset of the cantilever state) will lead to a short-lived signature $\Gamma_0\nu$ in the measured signal e. Assuming that the signature is negligible beyond M samples, $\Gamma_0 = [\Gamma_{0,1}, \Gamma_{0,2}, \ldots, \Gamma_{0,M}]^T$ can be determined analytically (see supplementary material[9] and Ref. 6), which will depend on the cantilever parameters ω_0, Q and the observer parameters ℓ_1 and ℓ_2. Γ_0 is not dependent on the initial condition mismatch ν, which can vary from impact to impact. Thus, if the cantilever does not interact with the sample, the signature $\Gamma_0\nu$ will be absent from the measured data $e = y - \hat{p}$ and is described by noise. If the cantilever does interact with the sample, e is described by $\Gamma_0\nu$ with an additive noise term. It can be shown that under the hypothesis H_0 of no interaction and under the hypothesis H_1 of an interaction of strength ν, the mismatch e between measured cantilever position y and its estimate $\hat{p}$ is described by

$$H_0 :\ e = \beta, \quad \text{and} \quad H_1 :\ e = \Gamma_0\nu + \beta. \tag{3}$$

Here, ν is a constant which depends on the strength of the impulsive impact of the cantilever with the sample (and thus the change in the cantilever state after impact), β is a Gaussian noise vector with statistics governed by the co-variance matrix $V = E\{\beta\beta^T\} = \sigma_\beta^2 I_M$. I_M is an identity matrix of size $M \times M$. Consider the function l (also termed the likelihood ratio) given by $\frac{1}{\sigma_\beta^2} e^T\Gamma_0$, which is a weighted (through V^{-1}) correlation of the the signal e with the dynamic profile Γ_0. Thus, l is large when a signature in the tracking error e aligned with Γ_0 appears. In absence of the signature, l behaves as Gaussian noise. Hence, presence or absence of a signature can be identified from the magnitude of l and the deviation from a zero mean process. Hence, under the hypotheses H_0 (feature not present) and H_1 (feature present), l is given by

$$H_0 :\ l = \frac{1}{\sigma_\beta^2}\beta^T\Gamma_0;\ H_1 :\ l = \frac{1}{\sigma_\beta^2}\nu\Gamma_0^T\Gamma_0 + \frac{1}{\sigma_\beta^2}\beta^T\Gamma_0. \tag{4}$$

The likelihood ratio under both hypotheses follows a normal distribution assuming ν is deterministic. Indeed, if $p(l;H_0)$ and $p(l;H_1,\nu)$ describe the conditional probability density functions (pdfs) of likelihood l under hypotheses H_0 and H_1, respectively, then $p(l;H_0) \sim \mathcal{N}(0,\sigma^2)$ and $p(l;H_1,\nu) \sim \mathcal{N}(l_\nu,\sigma^2)$ with $\sigma = \frac{1}{\sigma_\beta}\sqrt{\Gamma_0^T\Gamma_0}$ and $l_\nu = \frac{1}{\sigma_\beta^2}\nu\Gamma_0^T\Gamma_0$. The decision whether a feature is present or not is based on a threshold τ which is compared with the computed likelihood ratio $\ell_0 = \frac{1}{\sigma_\beta^2} e^T\Gamma_0$. If l_0 exceeds the threshold τ, a decision of

feature being present is made (decision H_1). Otherwise, feature is assumed to be absent (decision H_0).

The *fidelity* of the decision is defined as the conditional probability, $P(\text{Correct decision}|l = l_0)$, that the decision is correct given l_0 is an outcome of the random variable l. Clearly, $P(\text{Correct decision}|l = l_0) = P(H_1|l = l_0 > \tau)$ if $l_0 > \tau$ and $P(\text{Correct decision}|l = l_0) = P(H_0|l = l_0 \leq \tau)$ if $l_0 \leq \tau$. These probabilities can be determined analytically (see supplementary material) as follows:

$$P(H_1|l = l_0 > \tau) = \frac{g_1(l_0, \nu_0, \sigma)}{\exp\left(-\frac{l_0^2}{2\sigma^2}\right) + g_1(l_0, \nu_0, \sigma)}, \quad (5)$$

$$P(H_0|l = l_0 \leq \tau) = \frac{\exp\left(-\frac{l_0^2}{2\sigma^2}\right)}{\exp\left(-\frac{l_0^2}{2\sigma^2}\right) + g_1(l_0, \nu_0, \sigma)}, \quad (6)$$

with $g_1(l_0, \nu_0, \sigma) = \exp\left(-(l_0 - l_{\nu_0})^2/2\sigma^2\right)$. For determining the fidelity measure from (5) and (6), the strength of the impulsive impact ν_0 is needed which can be estimated using a least squares based method (using $e = \Gamma_o \nu_0 + \beta$) yielding

$$\hat{\nu} = (\Gamma_0^T \Gamma_0)^{-1} \Gamma_0^T e. \quad (7)$$

$\hat{\nu}$ is evaluated at the end of the last time window (which is M samples long), where the decision H_1 is made. $\hat{\nu}$ is used in the place of ν_0 in (5) and (6) for determining the fidelity measure. Expressions for the fidelity measure when the impact ν is described via a stochastic model are derived in supplementary material.

The efficacy of methods developed is evaluated using a piecewise-linear model of tip-sample interaction (Ref. 7); such a model captures many facets of typical tip-sample interactions although there are interactions that need different qualitative descriptions (see Ref. 8). In simulations, a cantilever with first mode resonant frequency $f_0 = 63.147$ kHz and quality factor $Q_0 = 227.849$ is used. Here, the external forcing $g(t)$ is a sinusoid with frequency f_0 with an amplitude that results in the cantilever to oscillate with an amplitude of 24 nm (with no interaction with the sample). The sample topography used in simulations is shown in Figure 2(a) which has only two kinds of features: one with a raised topography and the other with a lowered topography.

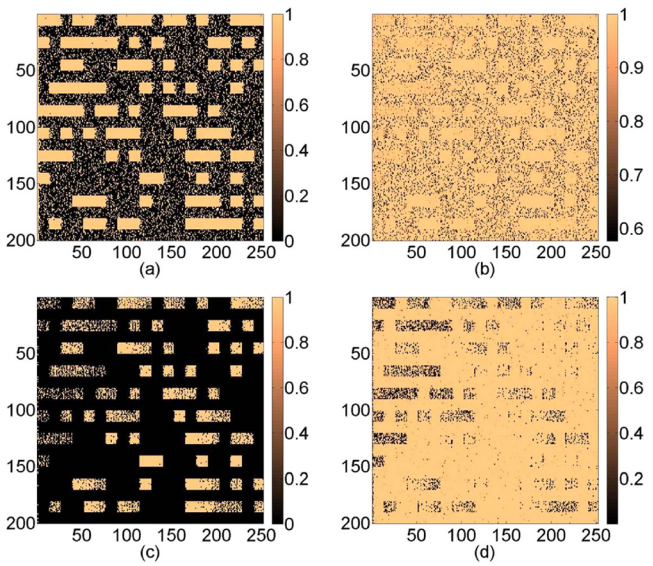

FIG. 3. Simulation results on decisions and corresponding fidelity measure for sample topography shown in Figure 2. (a) Decision image for a low threshold ($\tau = 0.3\tau_{mid}$). Decision values 0 and 1 imply absence and presence of high features respectively. Here, most high features are detected correctly with many detections of small untrue high features. (b) Fidelity value of the decision (shown in (a)) at each pixel; fidelity values are high where high features are truly present and small for the wrongly detected high features. (c) Decision image for a high threshold ($\tau = 1.6\tau_{mid}$). (d) Fidelity image corresponding to decisions made in (c). Here, absence of high features is decided with high confidence.

When interacting with the raised topography, the cantilever oscillations reach a steady-state with an amplitude of 22 nm. An observer given by (2) is used to generate the tracking error e. The signal e is processed, and the likelihood ratio $l = \frac{1}{\sigma_\beta^2} e^T \Gamma_0$ (see (4)) is obtained using a detection window of size $M = 28$. Here, the analog data are digitized using a sampling rate of 2 MHz. Fig. 2(a) shows the sample topography, and Fig. 2(b) shows the corresponding l value at each pixel. Given a threshold τ, if $l > \tau$, a decision of sample having a raised feature is made, otherwise, it is decided that the cantilever is at a valley. Fidelity is defined in terms of probability that the decision is correct and it is calculated for varying thresholds using (5) and (6). With a low threshold, presence of a feature will be detected with higher probability. However, it is also more likely that a feature's presence is detected even when there is none. $\tau_{mid} := \frac{\min(l)+\max(l)}{2}$ is the

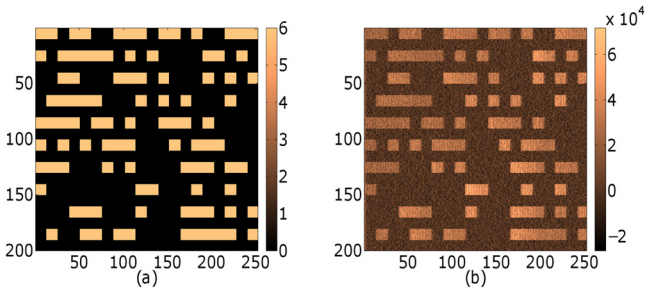

FIG. 2. (a) Sample topography used for simulation. The color bar indicates sample height in nm. (b) Value of the likelihood ratio at each pixel. Color bar specifies its range. y-axes for both images indicate index of the scan lines. Horizontal axes represent time in the unit of oscillation period $T_0 = 1/f_0 = 15.84$ ms.

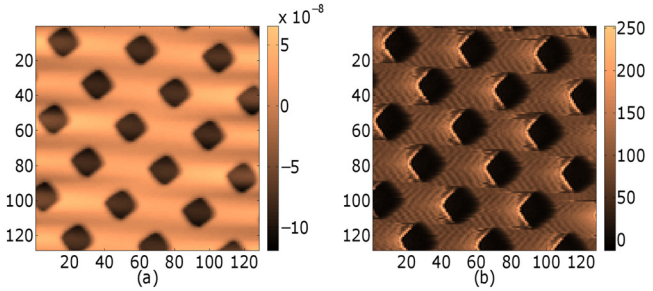

FIG. 4. (a) Height image of Silicon calibration sample taken with scan rate 1 Hz using MFP3D AFM from Asylum Research corresponding to 4 μm × 4 μm area. The color bar indicates height in meter. (b) Likelihood ratio l values at each pixel of (a) when imaged at scan rate of 31.25 Hz. The color bar specifies the range.

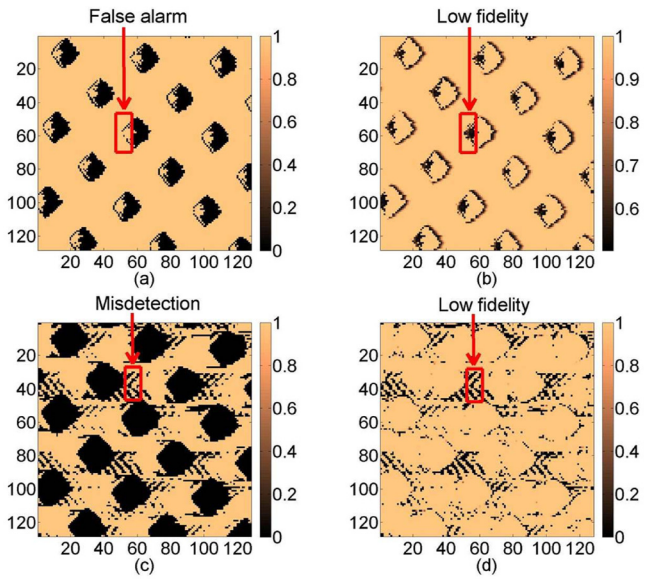

FIG. 5. (a) Decision image of silicon calibration sample for low thresholds obtained from experiments. Decision values 0 and 1 correspond to absence and presence of high topographic features. (b) Fidelity image. Low threshold ensures less missed detections of high topographic features. (c) Decision image of silicon calibration sample for relatively higher threshold obtained from experiments. (d) Fidelity image. High values of thresholds reduce detection of features with raised topography.

middle point of the range of values of l obtained from an image where τ values less than τ_{mid} are considered low thresholds and $\tau > \tau_{mid}$ are considered high. Figs. 3(a) and 3(b) show results when the threshold $\tau = 0.3\tau_{mid}$ is used. As the threshold is low, more features are declared being high features. Thus, most of the true high features are detected with the associated fidelity being high. However, many pixels are declared incorrectly as being high features (which appear as small bright dots), where the sample has a valley. Here, the fidelity image indicates that the imaging process should place low confidence on the decisions on these pixels. Figs. 3(c) and 3(d) show results when the threshold $\tau = 1.6\tau_{mid}$ is used. As the threshold is high, the decision rule declares less number of high features as high features, whereas absence of high features are easily detected. Thus, most of the pixels where there is a valley are correctly called. It is also seen that many true high features are wrongly detected as being valleys. Here, the fidelity image Fig. 3(d) indicates that the imaging process should place low confidence on the decisions on these pixels.

In the following, experimental results are presented where a MFP3D AFM manufactured by Asylum Research is used to scan a silicon grating sample with 1 μm by 1 μm pits of depth 100 nm. An Asylum Research AC240TS cantilever with first mode resonant frequency of 84.54 kHz and a quality factor of 254.18 is used. Fig. 4(a) shows the image of the sample taken at 1 Hz scan speed and serves as the reference image. The same sample is scanned at 31.25 Hz. The dither excitation and cantilever deflection data are gathered with 1 MHz sampling frequency. Fig. 4(b) shows the image of the likelihood ratio l. Similar to the simulation images, fidelity images are determined for different threshold values on decisions. Two such cases, one for low threshold $(\tau = 0.03\tau_{mid})$ and other for relatively higher threshold $(\tau = 0.7\tau_{mid})$ are shown in Fig. 5. Figs. 5(a) and 5(b) show results when the threshold $\tau = 0.03\tau_{mid}$ is used. Similar to the simulation results, as the threshold is low, more features are declared being high features. Thus, most of the true high features are detected with the associated fidelity being high. However, many pixels are declared incorrectly; small areas of pits are detected as having a flat topography where the sample has valleys. Here, the fidelity image indicates that the imaging process should place low confidence (low fidelity) on the decisions on these pixels. Figs. 5(c) and 5(d) show results when the threshold $\tau = 0.7\tau_{mid}$ is used. Here, the pit regions are correctly decided as valleys. However, regions on the flat portions of the sample are declared as being valleys (see Fig. 5(c)), which appear as black stripes in the image. The fidelity image in Fig. 5(d) determines that low confidence should be placed where the black stripes appear.

In conclusion, this letter reports a method to obtain in real-time a quantification of the fidelity of a binary (black and white) image obtained in dynamic mode operation of AFM. The experimental and simulation results demonstrate the efficacy of the fidelity imaging methodology presented. The work here lays the framework for extending the result to grayscale images and possibly for height imaging where confidence intervals on the height being measured can be provided.

We wish to acknowledge the support of the authors by Grants NSF-CCF 1116971 and NSF-ECCS 1202411.

[1]G. Binnig, C. Quate, and C. Gerber, Phys. Rev. Lett. **56**, 930 (1986).
[2]G. Haugstad, *Atomic Force Microscopy: Understanding Basic Modes and Advanced Applications* (John Wiley & Sons, 2012).
[3]R. Garcia and E. T. Herruzo, Nat. Nanotechnol. **7**, 217 (2012).
[4]S. Salapaka, A. Ramamoorthy, and M. Salapaka, IEEE Control Syst. **33**, 106 (2013).
[5]C.-T. Chen, *Linear System Theory and Design* (Oxford University Press, Inc., 1995).
[6]D. Sahoo, P. Agarwal, and M. Salapaka, in *American Control Conference, 2007. ACC'07* (IEEE, 2007), pp. 2135–2140.
[7]A. Sebastian, M. Salapaka, D. Chen, and J. Cleveland, J. Appl. Phys. **89**, 6473 (2001).
[8]Z. Parlak, Q. Tu, and S. Zauscher, Nanotechnology **25**, 445703 (2014).
[9]See supplementary material at http://dx.doi.org/10.1063/1.4905633 for detailed description of determining the observer dynamics under impulsive interaction and derivation of fidelity metrics.